Performance Analysis of a Medium-Power Helicon Thruster

Douglas D. Palmer[1] and Mitchell L. R. Walker[2]
High-Power Electric Propulsion Laboratory
Department of Aerospace Engineering
Georgia Institute of Technology, Atlanta, GA, 30332 USA
Phone: 404-385-2757
Fax: 404-894-2760

Marco Manete[3]
CISAS University of Padua Via Venezia 15 35131 Padova, Italy

Johan Carlsson[4]
Txcorp Boulder, Colorado USA

Cristina Bramanti[5], Daniele Pavarin[6]
Advanced Concept Team ESA ESTEC

A medium-power helicon thruster (MPHT) is an electric propulsion device that uses a helicon plasma source to achieve specific impulses of up to 1500 s with argon propellant.[1] The Center of Studies and Activities for Space (CISAS) has created a prototype design, and the Georgia Institute of Technology (GA Tech) has designed and built a nominally 1.5-kW MPHT that sustains high density, steady-state plasma over a range of operating conditions. All tests are performed in the GA Tech vacuum test facility at an operating pressure less than 3.1 x 10^{-5} Torr-Ar. Ion number density, electron temperature, and electron energy distribution function measurements are taken with an RF-compensated Langmuir probe as a function of RF frequency (2 – 15 MHz), RF forward power (0 – 1.5 kW), magnetic field strength (0 – 1100 Gauss), and argon mass flow rate (0.74 – 4.45 mg/s). The maximum ion number density is 8.0 x 10^{18} m^{-3}. The measurements are compared with several known helicon plasma sources. Experimental characterization of this device allows validation of the 1-D and 2-D codes developed at CISAS, which simulate plasma acceleration during vacuum expansion.

Nomenclature

A_p = Langmuir probe collection area
e = electron charge
I_{es} = electron saturation current
I_{sp} = specific impulse
k = Boltzmann constant
m_e = electron mass
n_i = ion number density
n_n = neutral number density
r_p = Langmuir probe collector radius

[1] Graduate Student Researcher, High-Power Electric Propulsion Laboratory, Department of Aerospace Engineering, 270 Ferst Drive, Atlanta, GA, 30332, Student Member AIAA.
[2] Assistant Professor, High-Power Electric Propulsion Laboratory, Department of Aerospace Engineering, 270 Ferst Drive, Atlanta, GA 30332, Member AIAA.

T_e = electron temperature
V_p = plasma floating potential
ω_{ic} = ion cyclotron frequency
ω_{ec} = electron cyclotron frequency

I. Introduction

Future deep-space missions require innovative propulsion systems that can fulfill mission life time requirements of decades or more. Chemical propulsion systems lack the performance to deliver the impulse for these missions. Current electric propulsion (EP) systems such as Hall effect thrusters (HETs) and ion engines possess the I_{sp} required for these missions, but are limited by the onboard power because the solar energy available diminishes as the vehicles moves away from the sun. Therefore, these vehicles will utilize other power sources, such as radioisotope generators (≤1 kW).

Recent mission designs suggest that the propulsion system may need to operate 90,000+ hrs.[2] To fully realize the benefits of an EP system, the thruster needs to operate for the entire duration of the mission at approximately 1 kW of input power. HETs life times fall well short of the required system life time due to channel insulator erosion. Demonstrated HET life times range from 2,000 hrs at 200-W up to 8,000 hrs at higher powers.[3-10] Recent advances in ion engine technology have increased life up to 30,000 hrs;[11] however, the life time is still limited by the hollow cathode electron source and electrode erosion. To achieve the near infinite life time requirements of future missions, the current EP failure mechanisms must be avoided.

Helicon plasma sources present an alternative to current propulsion systems as they are electrodeless EP systems with life times not limited by thruster components.[1, 12, 13] Helicon sources launch RF waves along an axial magnetic field to couple to the plasma.[1, 12-14] Ionization occurs within a closed insulator, which prevents erosion of the RF antenna as a failure mechanism. Helicon sources have been operated in cylindrical and staged configurations on argon, xenon, and many other propellants.[12-19] In each case, the majority of the plasma is confined to the center of the device due to the strong axial magnetic field. Recent investigations show that the Pyrex insulator experiences etch rates of zero for argon ion temperatures below 200 eV.[1] Ion acceleration by current-free double layers has observed in inductively-coupled plasmas driven by helical antennas under divergent magnetic fields.[1] The current-free double layer has the ability to produce an ion beam with a maximum velocity of 11.4 km/s. The ion beam separates from the device, which produces thrust.[1] To date, the thrust of a current-free double layer thruster has not been measured. Since electrodes and other system components do not contact the plasma, the failure modes of typical EP thrusters are not a factor. Thus, the helicon source may possess a nearly infinite operational life time.

The Center of Studies and Activities for Space (CISAS) has created a prototype medium-power helicon thruster (MPHT) design and the Georgia Institute of Technology (GA Tech) has designed and built a nominally 1.5-kW MPHT device that sustains high density, steady-state plasma over a range of operating conditions. The primary goal of this work is to measure the performance of the MPHT as a function of RF frequency (2 – 15 MHz), RF forward power (0 – 1500 W), magnetic field (0 – 1100 Gauss), and argon mass flow rate (1 – 4 mg/s). This work characterizes the MPHT device at significantly lower pressures than previous studies.[1, 20-22] A RF-compensated Langmuir probe is used to measure the ion number density, electron temperature, and electron energy distribution function (EEDF). In addition, there is a lack of simulation capability for helicon plasma sources. The secondary goal of this work is to gather experimental data on a known helicon source for use in validating 1-D and 2-D simulation codes developed by CISAS.

II. Experimental Setup

A. Facility

All experiments are performed in the Vacuum Test Facility (VTF), shown schematically in Fig. 1. The VTF is a stainless steel vacuum chamber that has a diameter of 4 m and a length of 7 m. Two 3800-CFM blowers and two 495-CFM rotary-vane pumps evacuate the facility to moderate vacuum (30 mTorr). To reach high-vacuum (10^{-7} Torr), the VTF employs six 48" diffusion pumps, with a combined nominal pumping speed of 600,000 l/s on air, 840,000 L/s on hydrogen, and 155,000 l/s on xenon. The VTF pumping speed is varied by changing the number of diffusion pumps in operation. The combined pumping speed of the facility is 600,000 l/s on air and with a base pressure of 1.2×10^{-4} Pa (9.5×10^{-7} Torr).

A Varian model UHV-24 ionization gauge with a Varian senTorr vacuum gauge controller monitors the chamber pressure. The UHV-24 ionization gauge is calibrated for air by the manufacturer. The ionization gauge measures pressure over the range of 10^{-2} Pa (10^{-4} Torr) to 10^{-10} Pa (10^{-12} Torr) with an accuracy of ±20% as reported by Varian. The VTF also utilizes a tubulated Kurt J. Lesker Company (KJLC) model G100TF ionization gauge with a KJLC model IG2200 ionization gauge controller, and a KJLC Accu-Quad residual gas analyzer (RGA), both located on the top of the chamber. The RGA has a detection limit of 5 x 10^{-14} Torr, and an accuracy of ±10% as reported by KJLC.

Table 1 shows the VTF operating pressure for each flow rate. Previous investigations show these pressures are lower than typical pressures for helicon experiments.[1, 13, 23] The chamber pressures listed are the indicated pressures from the RGA.

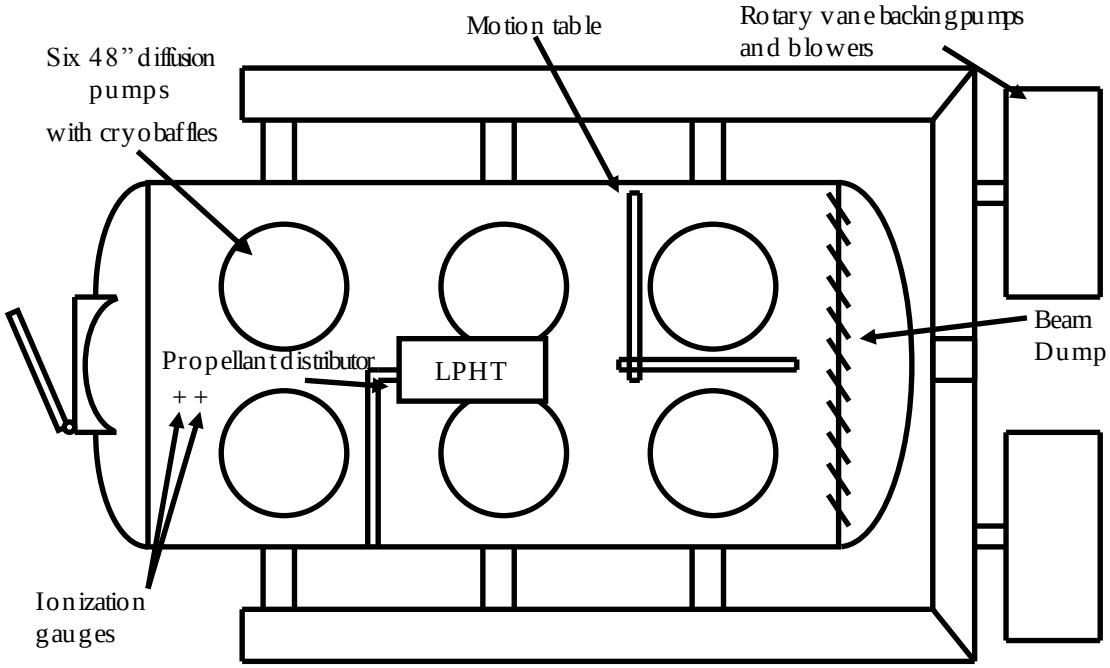

Figure 1. Schematic of Vacuum Test Facility.

B. Medium-Power Helicon Thruster

Figure 2 shows the MPHT used in this experiment. Figure 3 shows a schematic of the medium-power helicon thruster RF power, solenoid, and mass flow system. The plasma is insulated by a 45 mm diameter, 600 mm long Pyrex glass tube. A 132.8 mm long by 49 mm diameter copper left-helical pitch antenna is wrapped around the tube. The antenna hangs freely on a separate support system with two copper rods of 9.52 mm diameter to prevent thermal interference with thrust measurements. The power leads to the antenna as well as the solenoids are EMF shielded with tinned copper mesh to minimize RF radiation.

High purity (99.9995% pure) argon or xenon gas is fed through an MKS 1179JA mass flow controller through stainless steel feed lines to the propellant distributor. A custom fixed volume mass flow calibration system is employed to ensure proper flow rates from the mass flow controller. The mass flow controller has an accuracy of ±1% of full scale.

The solenoid generates a steady-state axial magnetic field up to 1100 Gauss. The solenoid is powered by a 60-kW EMHP DC power supply. ½" and ¼" diameter ferrites reduce RF signal propagation up the solenoid power leads. RF power is provided to the antenna via the RF power system. The RF power input lead connects at the downstream end of the helical antenna and the return leads connect at the upstream end. This configuration yields the best coupling to the plasma.[12]

Table 1. Operating pressures for mass flow rates of argon.

Mass flow rate (mg/s)	**Operating Pressure** (Torr-Ar)
0.5	2.0 x 10^{-5}
1.5	2.4 x 10^{-5}
2.5	2.7 x 10^{-5}
3.0	3.0 x 10^{-5}

The Acom 2000A linear amplifier produces RF power up to 1500 W steady state. The RF forward and reflected power levels are measured with a Bird 43 Thruline wattmeter and the Palstar AT5K matching network internal power gauge. The Bird 43 Thruline wattmeter has an accuracy of ±5% of full scale, while the Palstar AT5K wattmeter has an accuracy of ±10% of full scale. The Palstar AT5K 3500-W L-Type matching network, which has a native impedance of 50 Ω, matches the impedance of the amplifier to the load. The impedance of the antenna is extremely low, which means little inductive reactance is present. For this antenna configuration, the resistance is approximately 1 Ω without plasma present. To minimize radiation outside of the antenna and ionization chamber, *i.e.*, reduce reflected and lost power, the impedance of all cabling and feedthroughs is 50 Ω. In addition, a standard fixed distance is maintained between all conductors. The RF reflected power is less than 1% of the forward power for all measurements taken, which indicates that the matching network is well-tuned to the antenna.

The RF power system is enclosed in a Faraday cage to prevent RF radiation from the system components. The cabinet is cooled through EMI shielded vents and is grounded to the vacuum chamber.

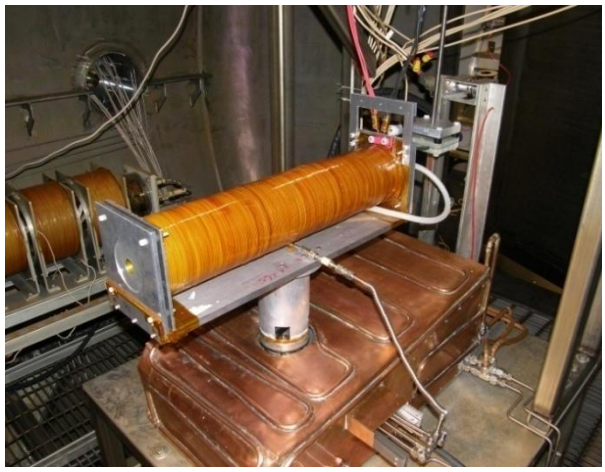

Figure 2. Medium-power helicon thruster mounted on thrust stand.

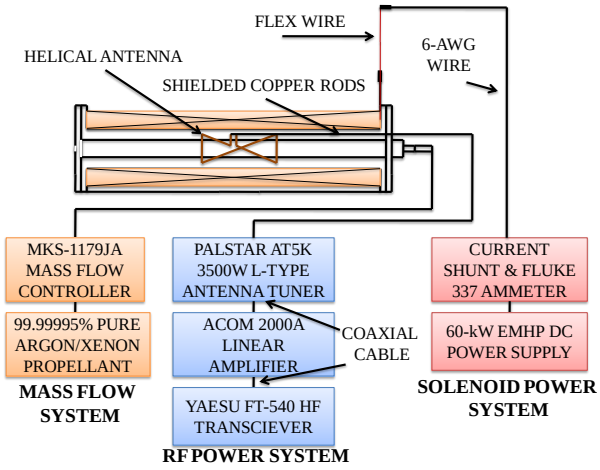

Figure 3. Schematic of MPHT subsystems.

C. Hiden Analytical Langmuir Probe

All ion number density, electron temperature, and EEDF measurements are taken with the Hiden ESPION Langmuir probe system. Chen shows this system is suitable for use in high-density magnetized RF plasma measurements.[18, 24, 25] Figure 4 shows the Hiden ESPION system. The probe has an error of ±50% for electron number density and ±20% for electron temperature.[24] The probe is mounted to a 1.5 m by 1.5 m Parker Daedel automated motion control system to provide linear axial and radial motion with an accuracy of ±1 μm. The probe features a compensation electrode tuned to remove RF signals throughout the 2 – 15 MHz RF frequency range used in these tests. This corrects measurements for changes in the plasma potential relative to the system ground potential.[26] Chen recommends the use of very thin probes, where the probe tip radius is no larger than three times the Debye length, so that Orbital-Motion Limited (OML) theory may be used.[18] In this work, a 0.15 mm diameter by 10 mm long tungsten probe tip is used as the collector filament. The collector filament is mounted to the end of an 810 mm long ceramic sting, which contains the RF-compensation inductors. The inductors are cooled through the umbilical with a forced air system. A reference electrode positioned behind the collector filament provides a return path for current collected from the plasma. The Hiden software, connected to the control head, collects I-V curves from the plasma. Figure 5 shows a sample Langmuir probe I-V trace. All diagnostic equipment is grounded to its own separate ground within the facility to prevent RF interference in the measurements.

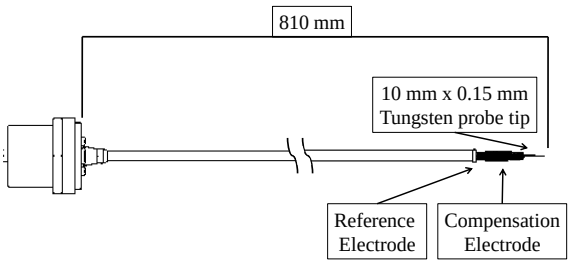

Figure 4. Schematic of the Hiden ESPION Langmuir probe.

1. Langmuir Probe Theory

The Hiden ESPION system contains a data analysis tool that uses OML and the Allen, Boyd and Reynolds analysis techniques. OML theory assumes that the ion collection current is independent of the plasma potential, and that the collection current is only limited by the angular momentum of the ions about the probe. Furthermore, there exists a sheath edge outside of which the energy distribution is Maxwellian.[26] Figure 6 shows a schematic of the OML sheath and an absorption boundary.[25] OML theory provides a simple relationship for ion current. Eqn. (1) shows this relationship.[25]

$$I \xrightarrow[T_i \to 0]{} A_p n e \frac{\sqrt{2}}{\pi} \left(\frac{|eV_p|}{M} \right)^{1/2} \tag{1}$$

To analyze the raw I-V data, the square root of the ion current fit is added to the original I-V curve to obtain a characteristic, which consists of electron current only.[26] The natural logarithm of the electron current is calculated and plotted against the bias voltage. Eq. 2 calculates the electron temperature by fitting a line to the linear transition region.[25] The relationships for electron temperature and electron number density are shown in Equations (2) and (3).[26]

$$T_e = \frac{-1}{slope(I)} \tag{2}$$

$$n_e = 3.73x10^{13} \frac{I_{es(amps)}}{A_{p(m^2)} \sqrt{T_{e(eV)}}} \tag{3}$$

2. Druyvesteyn Method for EEDF Calculation

The Druyvesteyn method is used to calculate the EEDF from the I-V characteristics. The Druyvesteyn method observes that the second derivative of the electron current with respect to the probe potential is proportional to the electron energy distribution function if the velocity distribution is isotropic. Eq. 4 shows this relationship.[27]

$$f_e(E) = \frac{-4}{A_p e^2} \left(\frac{m_e (V_{plasma} - V)}{2e} \right)^{1/2} \frac{d^2 I_e}{dV^2} \tag{4}$$

If the EEDF is Maxwellian, Eq. 4 can be integrated twice to give the theoretical electron current as a function of probe voltage below the plasma potential. Eq. 5 shows the result of these integrations.[27]

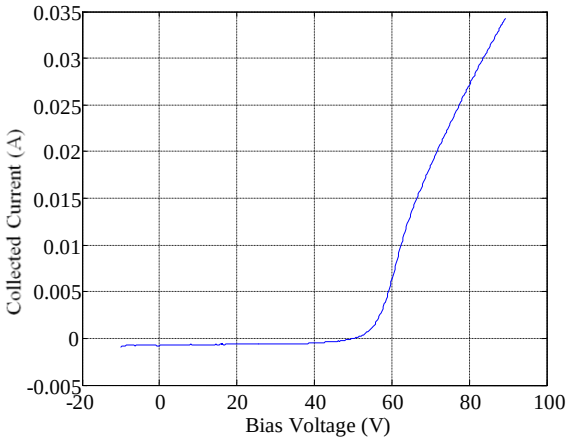

Figure 5. Measured I-V characteristic on argon propellant.

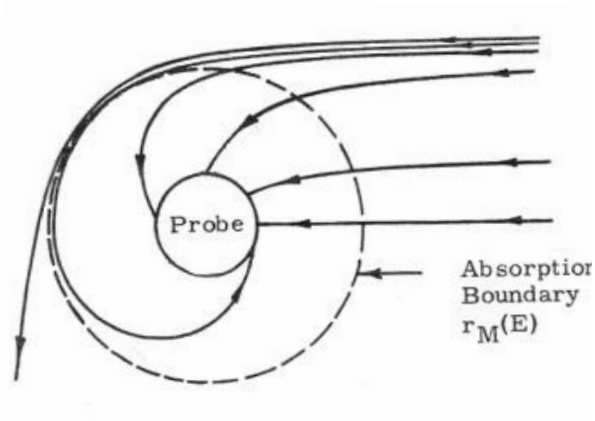

Figure 6. OML theory electron motion near a positively-biased Langmuir probe.[25]

$$I_e(V) = \left(eA_p N \sqrt{\frac{kT_e}{2\pi m_e}} \right) \exp\left(\frac{-e(V_{plasma} - V)}{kT_e} \right) \quad (5)$$

The calculation of the EEDF is performed automatically in the Hiden software, and is accurate to ±50%.[26] The second derivative method requires a smooth I-V trace to produce accurate results.[27] Any increases in the second derivative can produce false peaks in the EEDF. To allow numerical integration, each I-V trace is taken at 0.1 V resolution from -15 V to 90 V. Ten I-V traces per operating point are collected and the average of the ten traces is used as an input to the Druyvesteyn method. The EEDF is smoothed by averaging ten I-V curves per measurement, and then using a 25 point smoothing filter on the average. This method of data analysis is supported by Hiden.[26] The EEDF contained outlying points above 10 eV, however these are on the order of 2% of the peak value and are a result of numerical integration. These values are removed from the results.

III. Experimental Data

The MPHT is operated over a range of conditions in order to characterize the device. Axial profiles are taken to determine the plasma ion number density and electron temperature along the device centerline. The axial profiles are useful to determine if ions are exiting the device and separating from the thruster.[1] Shifts in the ion saturation current as RF power changes are used to indicate mode shifts in the plasma.[19] Measurements of the ion number density and electron temperature are taken as a function of power to determine what power levels are required to obtain a given mode at several magnetic field strengths. Measurements of the ion number density and electron temperature are taken as a function RF frequency to determine if an optimal frequency exists that maximizes ion number density. For the data presented, the propellant distributor is located at an axial location of 0 mm. The center of the antenna is at an axial location of 350 mm. The device exhaust is at an axial location of 600 mm.

A. Axial Profile

Figures 7 and 8 show the ion number density and electron temperature as a function of axial location for argon propellant. These measurements are taken along the centerline of the device, beginning 30 mm from the propellant distributor. Figures 7 and 8 show that at 1 kW of forward power, the 1100 Gauss magnetic field case achieves the maximum ion number density of 7.9 x 10^{18} m^{-3}. The zero Gauss and 500 Gauss cases have significantly lower ion number densities, with a peak value of 1.8 x 10^{18} m^{-3}. The ion number densities increase as the plasma moves downstream, however there is a significant neutralization at the exhaust, which decreases the ion number density to 4.1 x 10^{16} m^{-3}. In the plume, ion number density decreases rapidly, reaching at 1.1 x 10^{15} m^{-3} at an axial location of 675 mm (75 mm into the plume). Electron temperatures are highest in the zero Gauss setup, peaking at 5.8 eV. The minimum electron temperature recorded is in the 500 Gauss case, at 1.2 eV. Electron temperatures show no clear

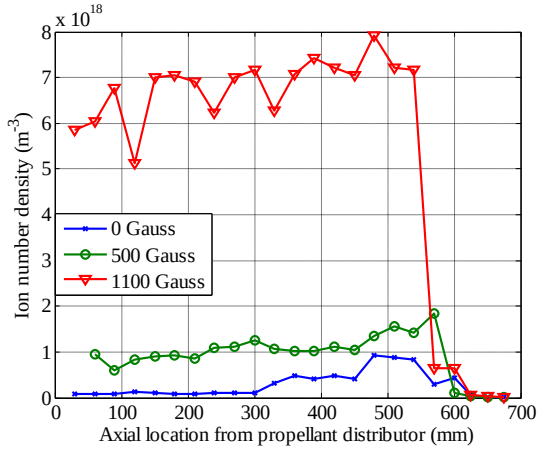

Figure 7. Ion number density versus axial location, along channel centerline. *7 MHz RF frequency, 1 kW RF forward power, 3 mg/s Ar mass flow rate, 3.0 x 10^{-5} Torr-Ar operating pressure.*

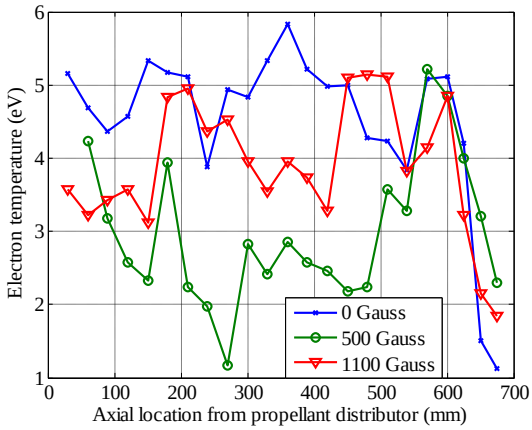

Figure 8. Electron temperature versus axial location, along channel centerline. *7 MHz RF frequency, 1 kW RF forward power, 3 mg/s Ar mass flow rate, 3.0 x 10^{-5} Torr-Ar operating pressure.*

trend, however all cases show a significant decrease in electron temperature at the exhaust plane and in the plume. The zero Gauss case reaches an electron temperature of 1.1 eV, while the 500 Gauss case reaches 2.3 eV.

B. RF power profile

Figures 9 and 10 show the dependence of ion number density and electron temperature on RF forward power at several magnetic field strengths for argon propellant. These measurements are taken at an axial location of 350 mm, which is directly under the antenna centerline. The ion number density is relatively constant with RF forward power at low magnetic field strengths, with values ranging from 1.1 x 10^{17} m^{-3} to 9.6 x 10^{17} m^{-3}. Above 500 Gauss, the ion number density increases rapidly with RF forward power, jumping to a peak value of 7.7 x 10^{18} m^{-3} at an RF power of 1400 W. The 750 Gauss and 1100 Gauss cases both have the large jump in ion number density at an RF power of 800 W. The electron temperature decreases as the strength of the magnetic field increases. The 1100 Gauss has minimum electron temperature of 2.1 eV, while the zero Gauss case achieves the maximum of 6.2 eV.

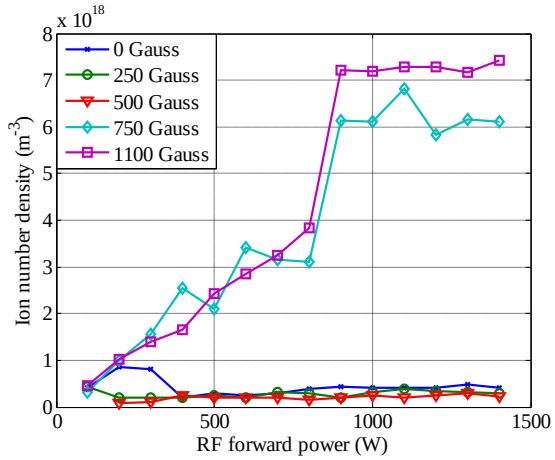

Figure 9. Ion number density versus RF forward power. *, 350 mm axial location, 7 MHz RF frequency 3 mg/s Ar mass flow rate, 3.0 x 10^{-5} Torr-Ar operating pressure.*

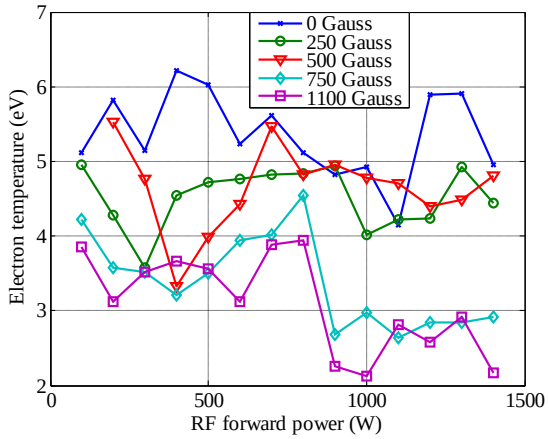

Figure 10. Electron temperature versus RF forward power. *350 mm axial location, 7 MHz RF frequency, 3 mg/s Ar mass flow rate, 3.0 x 10^{-5} Torr-Ar operating pressure.*

C. RF frequency profile

Figures 11 and 12 show the ion number density and electron temperature measured as a function of RF frequency at two RF forward power levels. Each measurement is taken at 1100 Gauss magnetic field, at a location 350 mm upstream of the exhaust plane for argon propellant. Figures 11 and 12 show that between 6 and 8 MHz, as

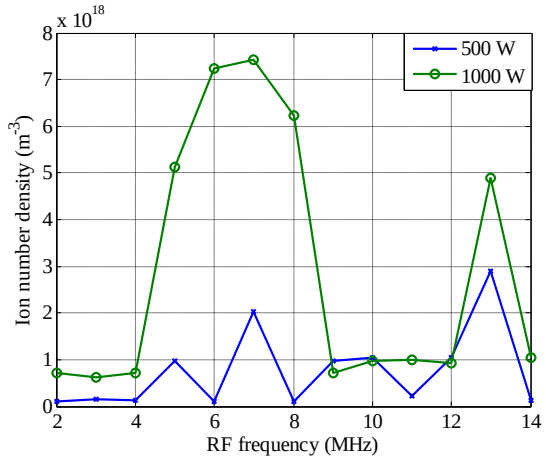

Figure 11. Ion number density versus RF frequency. *350 mm axial location, 1100 Gauss B-field, 3 mg/s Ar mass flow rate, 3.0 x 10^{-5} Torr-Ar operating pressure.*

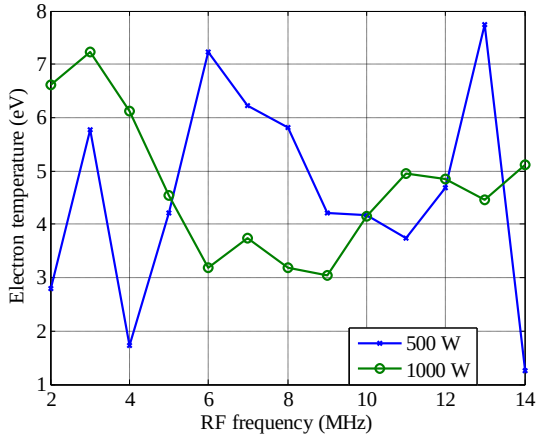

Figure 12. Electron temperature versus RF frequency. *350 mm axial location, 1100 Gauss B-field, 3 mg/s Ar mass flow rate, 3.0 x 10^{-5} Torr-Ar operating pressure.*

well as 13 MHz are good coupling frequencies for this propellant. The peak ion number density of 7.4 x 10^{18} m^{-3} occurs at 7 MHz RF frequency. At 500 W RF power, the optimal frequency to maximize ion number density is 13 MHz.

D. Electron Energy Distribution Function

Figure 13 shows the EEDF at several selected RF frequencies. These measurements are taken at an axial location of 350 mm, on channel centerline, at a magnetic field strength of 1100 Gauss. This location is directly underneath the antenna. Figure 13 shows that the EEDF peak value and width vary with RF frequency. The peak of the EEDF varies between a minimum of 2.5 eV for the 12 MHz case to a maximum of 5.6 eV for the 7 MHz case. The 7 MHz, 10 MHz, and 11 MHz cases show a small number of low energy electrons.

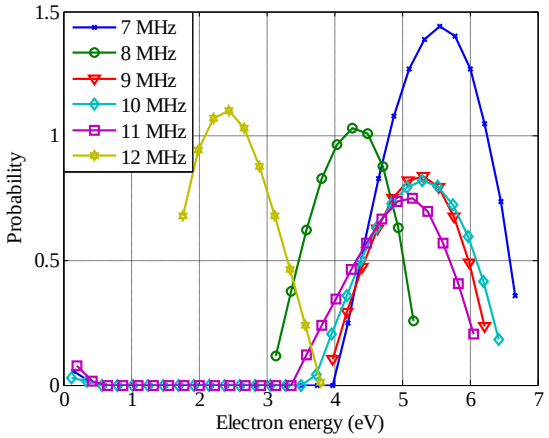

Figure 13. EEDF at several selected RF frequencies. *1 kW RF forward power, 1100 Gauss magnetic field, 3 mg/s Ar mass flow rate, 350 mm axial location, 3.0 x 10^{-5} Torr-Ar operating pressure.*

IV. Discussion

The RF-compensated Langmuir probe measurements are now analyzed to determine the trends in plasma properties across the operating conditions measured, and the ability of the thruster to operate in the low and medium power configurations as predicted by CISAS theory. In order to understand the mechanisms behind the trends indicated in the measurements, plasma parameters are calculated for each trend. These include the electron and ion cyclotron frequencies ω_{ic},and ω_{ec}, and plasma parameter Λ. The gyroradii calculations for measurements with argon indicate the electrons are magnetized for all the magnetic field cases, but the ions are not. Table 2 shows the electron and ion cyclotron frequencies calculated from the RF power ion number density and electron temperature profiles shown in Figures 8 and 9. The plasma parameter, which is a measure of the population of the Debye sphere, is calculated to be on the order of 10^{-24} for all measurements taken. This indicates the Debye sphere is sparsely populated, corresponding to strongly coupled plasma.[17]

Table 2. Electron and ion cyclotron frequencies.

	100 Gauss	250 Gauss	500 Gauss	750 Gauss	1100 Gauss
Electron cyclotron frequency (Hz)	1.8 x 10^{9}	4.4 x 10^{9}	8.8 x 10^{9}	1.3 x 10^{10}	1.9 x 10^{10}
Ion cyclotron frequency (Hz)	2.4 x 10^{4}	6.0 x 10^{4}	1.2 x 10^{5}	1.8 x 10^{5}	2.7 x 10^{5}

Figures 7 and 8 show the ion number density and electron temperature as a function of axial location within the device. The 1100 Gauss magnetic field case has an 85% higher ion number density than the 500 Gauss and zero Gauss cases, peaking at 7.8 x 10^{18} m^{-3}. This indicates the 1100 Gauss magnetic field case is in a different coupling mode than the 500 and zero Gauss cases, and since the magnetic field induces the increase, the mode is likely a helicon mode. Each profile has a large drop in ion number density at the exhaust of the device, accompanied by a large decrease in the electron temperature. Thus, there is a mechanism that not only causes ion recombination, but also removes energy from the electron population. There is an aluminum diaphragm at the exhaust of the device that is electrically isolated from ground. It is possible that the ions recombine at the aluminum diaphragm, either by mechanical, *i.e.*, choking the flow, or electrical means. Plume measurements indicate the high density plasma does not exit the device. West has shown more gradual trends in ion number density, which indicate this rapid discontinuous decrease in ion number density may prevent a current-free double layer from forming in the divergent magnetic field at the exhaust.[1] Furthermore, secondary electron emission from the aluminum diaphragm may lower the bulk electron temperature. Figure 14 shows the axial and radial magnetic field strengths as a function of axial location. The magnetic field diverges as the axial location increases towards the exhaust. Without a double layer present, only marginal thrust will be produced by the device, therefore the mechanism behind the ion number density and electron temperature decrease must be investigated.

Figures 9 and 10 show the ion number density versus RF forward power. These profiles indicate a large jump in ion number density at an RF forward power of 800 W, for magnetic fields stronger than 750 Gauss. The ion number density increases from 3.9 x 10^{18} m^{-3} to 7.3 x 10^{18} m^{-3} for the 1100 Gauss case. The large increase in ion number density at this condition can be interpreted as a shift to a helicon wave mode, since the magnetic field strength is a prerequisite to this rise. The ion number density jump at 800 W is accompanied by an electron temperature decrease, which matches theory. At low magnetic fields, the ion number density is independent of RF forward power. This indicates capacitive coupling, which is supported by the fact that for capacitive coupling, the densest plasma will occur directly at the antenna.[19] While RF power is not reflected back up the lines, this power must be dissipated if it is not used to ionize propellant or heat electrons. This energy is most likely radiated away to the vacuum chamber walls. For the 750 Gauss and 1100 Gauss cases, trends in ion number density indicate a shift to inductive coupling, followed by jumps to helicon modes. Many investigations show that inductive plasmas have linear increases in ion number density, followed by a large jump in ion number density as the devices shifts to helicon mode.[1, 13, 14, 16, 19] Figure 10 shows that the electron temperature reaches high values at low RF power settings, however once a new power coupling mode is reached, the electron temperatures decrease because the device no longer uses large amounts of power to heat electrons.[12, 20] A high ion number density with cold electrons is optimal for a propulsion device, because this minimizes the energy is lost heat electrons, and maximizes the number of ions available for acceleration.

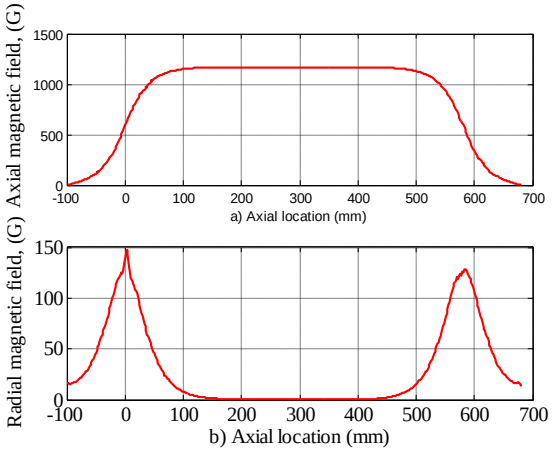

Figure 14. Axial and radial magnetic field versus axial location. *Radial location of 20 mm, at the Pyrex insulator. The propellant distributor is located at an axial location of 0 mm. The center of the antenna is at an axial location of 300 mm. The exit plane of the device is at an axial location of 600 mm.*

Figures 11 and 12 show the ion number density and electron temperature as a function of RF frequency. The ion number density increases sharply from 5 to 8 MHz, and again at 13 MHz. For argon propellant in this device, measurements indicate 8 MHz to be the optimal frequency to maximize the ion number density. 14 MHz is the best frequency for minimization of electron temperature, while 13 MHz maximizes electron temperature. The 1000 W RF forward power case shows a very large jump in ion number density at the above frequencies, while the 500 W case has a much more constant trend with RF frequency. This indicates that 1000 W of RF power excites a different coupling mode within the plasma. This mode is most likely a helicon wave mode as the densities reached match the wave modes seen in Figure 9, which require the magnetic field.

Figure 13 shows the EEDF at several selected RF frequencies. As predicted, the shape and peak of the EEDF varies by selection of RF frequency.[29] The peak in the EEDF varies as low as 2.6 eV to as high as 5.8 eV based on the frequency selected between 7 and 12 MHz for this device. In two cases, 10 and 11 MHz, there are low energy electrons observed below 0.5 eV in the EEDF. Figure 13 shows at 7 MHz RF frequency, there is a higher probability of electron energies within the indicated range (4 – 6.6 eV) than all the other frequencies. Figures 11 and 12 show ion number density correlates with the relative probabilities in Figure 13, *i.e.*, increases in the relative probability of the EEDF at that frequency correspond to increases in ion number density.

Figure 15 shows the electron-argon ionization cross section over the range of electron temperatures measured. This may be related to the EEDF peak value and probability distribution. In this case, the peak electron energy is from the 7 MHz case, while the minimum is from the 12 MHz case. The 7 MHz case corresponds to a much larger electron-argon collisional cross section than the 12 MHz case, and therefore should produce a higher number density if at the same operating condition and

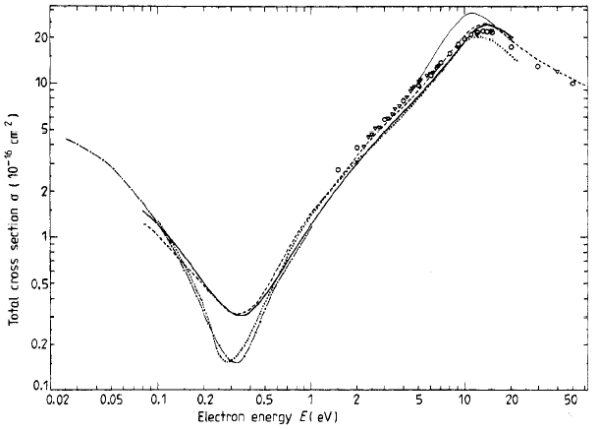

Figure 15. Electron-argon ionization cross section versus electron energy.[28]

same coupling efficiency, which it does. In this case, the increase in collisional cross section from 2.4 x 10^{-16} cm^2 to 8.1 x 10^{-16} cm^2 (+237%) results in an increase in ion number density from 9.8 x 10^{-16} m^{-3} to 7.5 x 10^{-17} m^{-3} (665%). While most of the plasmas are strongly coupled according to the plasma parameter Λ, the coupling may not be exactly the same in each case.

Conclusion

The maximum ion number density measured is 8.0 x 10^{18} m^{-3}, which occurs at an operating condition of 7 MHz RF frequency, 1000 W of RF forward power, 1100 Gauss magnetic field, 3 mg/s argon, at an axial location 500 mm downstream of the propellant distributor. It is experimentally verified that the RF is coupling to the magnetic field to produce a jump in ion number density, accompanied by a decrease in electron temperature. The ion number density decreases rapidly at the exhaust plane. The RF power profiles measured indicate a jump to a helicon wave mode, as magnetic field strength increases above 750 Gauss. In this mode, the ion number density increases while the electron temperature decreases, which is optimal for thrust production. The RF frequency profiles indicate 7 MHz is the ideal frequency when operating at 1000 W RF power and 1100 Gauss magnetic field strengths, while at 500 W RF power there is no apparent optimal frequency to maximize the ion number density. The magnetic field at the exhaust is divergent and appropriate for double layer formation, however double layer formation may be prevented by a rapid decrease in ion number density at the exhaust, as a result of a diaphragm at the exhaust plane.[1, 20-22] The MPHT is capable of operating in the low and medium power regimes as required to validate the 1-D and 2-D CISAS codes.

Acknowledgments

The authors wish to thank the Marshall Space Flight Center for supplying the RF power system and Scott Elliott and Scott Moseley of the Georgia Tech Aerospace Engineering Machine Shop for fabrication of the hardware.

References

1. West, M., Charles, C., Boswell, R., "Testing a Helicon Double Layer Thruster Immersed in a Space-Simulation Chamber," Journal of Propulsion and Power, Vol. 24, No. 1, Jan. - Feb., 2008, pp.134-141.
2. Schreiber, J.G., "Capabilities and technical issues regarding the Stirling radioisotope generator," Aerospace Conference Proceedings, IEEE, Vol. 5, No. 1, 2002, pp.5-2445 - 5-2452.
3. Manzella, D., Oh, D., Aadland, R. "Hall Thruster Technology for NASA Science Missions," AIAA-2005-3575, *41st Joint Propulsion Conference and Exhibit*, Tuscon, AZ, July 10-13, 2005.
4. Cheng, S.Y., Martinez-Sanches, Manuel. "Modeling of Hall Thruster Lifetime and Erosion Mechanisms," IEPC-2007-34, *30th International Electric Propulsion Conference*, Florence, Italy, Sep. 17-20, 2007.
5. Jankovsky, R.S., Jacobson, David T., Sarmiento, Charles J., Pinero, Luis R., Manzella, David H., Hofer, Richard R., Peterson, Peter Y. "NASA's Hall Thruster Program 2002," AIAA-2002-3675, *38th Joint Propulsion Conference and Exhibit*, Indianapolis, IN, July 7-10, 2002.
6. Fisch, N.J., Raitses, Y. , Litvak, A. A., Dorf, L. A. "Segmented Electrode Hall Thruster Operation in Single and Two Stage Regimes," IEPC-99-101, *26th International Electric Propulsion Conference*, Kitakyushu, Japan, Oct. 17-21, 1999.
7. Fisch, N.J., Raitses, Y., Litvak, A. A., "Variable Operation of Hall Thruster with Multiple Segmented Electrodes," Journal of Applied Physics, Vol. 89, No. 4, Feb., 2001, pp.2040-2046.
8. Fruchtman, A., Fitsch, N. J., Raitses, Y. . "Hall Thruster with Absorbing Electrodes," AIAA-2000-3659, *36th Joint Propulsion Conference and Exhibit*, Huntsville, AL, July 16-19, 2000.
9. Szabo, J., Warner, N., Martinez-Sanchez, M. "Instrumentation and Modeling of a High Specific Impulse Hall Thruster," AIAA-2002-4248, *38th Joint Propulsion Conference and Exhibit*, Indianapolis, IN, July 7-10, 2002.
10. Zhurin, V.V., Kaufman, H. R., Robinson, R. S., "Physics of Closed Drift Thrusters," Plasma Sources Science and Technology, Vol. 8, No. 1, Feb., 1999, pp.R1-R20.

11. Sengupta, A., et al. "Status of the Extended Life Test of the Deep Space 1 Flight Spare Ion Engine after 30,000 hours of Operation," AIAA-2003-4558, *39th Joint Propulsion Conference and Exhibit*, Huntsville, AL, July 20-23, 2003.
12. Chen, F.F. "Helicon Wave Plasma Sources," *Proceedings of the International Conference on Plasma Physics*, Kiev, USSR, 1987.
13. Chen, F.F., "Plasma Ionization by Helicon Waves," Plasma Physics and Controlled Fusion, Vol. 33, No. 4, 1991, pp.339-364.
14. Palmer, D., Akinli, C., Walker, M. L. R. "Characterization of an Annular Helicon Plasma Source," IEPC-2007-202, *30th International Electric Propulsion Conference*, Florence, Italy, September 17-20, 2007.
15. Beal, B.E., Gallimore, A. D., Morris, D. P., Davis, C., Lemmer, K. M. "Development of an Annular Helicon Source for Electric Propulsion Applications," AIAA-2006-4841, *42nd Joint Propulsion Conference and Exhibit*, Sacramento, CA, July 8-11, 2006.
16. Palmer, D., Walker, M. L. R. "Operation of an Annular Helicon Plasma Source," AIAA-2008-4926, *42nd Joint Propulsion Conference and Exhibit*, Hartford, CT, July 21-24, 2008.
17. Chen, F.F., *Plasma Physics and Controlled Fusion*. 2 ed. Vol. 1. 1983, New York: Springer Science.
18. Chen, F.F. Use of Langmuir probes in RF plasmas. *INER*. 2008. Taiwan.
19. Chi, K.-K., Sheridan, T. E., Boswell, R. W., "Resonant cavity modes of a bounded helicon discharge," Plasma sources Science and Technology, Vol. 8, No. 3, 1999, pp.421-431.
20. Charles, C., Boswell, R. W., "Current-Free Double Layer Formation in a High Density Helicon Discharge," Applied Physics Letters, Vol. 82, No. 9, 2003, pp.1356-1358.
21. Charles, C., "A Review of Recent Laboratory Double Layer Experiments," Plasma Sources Science and Technology, Vol. 16, No. 4, 2007, pp.R1-R25.
22. Plihon, N., Chabert, P., Corr, C. S., "Experiment Investigation of the Double Layers in Expanding Plasmas," Physics of Plasmas, Vol. 14, No. 013506, 2007, pp.1-16.
23. Randolph, T., Kim, V., Kaufman, H., Kozubsky, K., Zhurin, V. V., Day, M. ""Facility Effects on Stationary Plasma Thruster Testing"," IEPC-93-093, *23rd International Electric Propulsion Conference*, Seattle, WA, Sep. 13-16, 1993.
24. Chen, F.F., "Langmuir probe analysis for high density plasmas," Physics of Plasmas, Vol. 8, No. 6, 28 February, 2001.
25. Chen, F.F. "RF Langmuir Probes, revisited," *58th Gaseous Electronics Conference*, San Jose, CA, 2005.
26. *Handbook of Plasma Diagnostics*,
27. Herman, D., "The Use of Electrostatic Probes to Characterize the Discharge Plasma Structure and Identify Discharge Cathode Erosion Mechanisms in Ring-Cusp Ion Thrusters," Ph.D. Thesis, The University of Michigan, Dept. of Aerospace Engineering, Ann Arbor, MI, 2005
28. Ferch, J., Granitza, B., Masche, C.,Raith, W., "Electron-argon total cross section measurements at low energies by time-of-flight spectroscopy," Journal of Physics B, Vol. 18, No. 5, 1985, pp.967-983.
29. Shoji, T., Mieno, Tetsu, Kadota, Kiyoshi. "Control of Energy Distribution of Electrons and Hydrocarbon Film Deposition by Whistler Wave Discharge," *International Seminar on Reactive Plasmas*, Nagoya, Japan, 1991.